Macromolecular Research

Article

DOI 10.1007/s13233-017-5158-x

www.springer.com/13233 pISSN 1598-5032 eISSN 2092-7673

Hierarchical Structured, Nitrogen-Incorporated Graphene Aerogel for High Performance Supercapacitor

Xu Yu[1,2]
Manikantan Kota[1]
Ho Seok Park*[,1]

[1] School of Chemical Engineering, Sungkyunkwan University, 2066, Seobu-ro, Jangan-gu, Suwon-si, Gyeonggi 16419, Korea
[2] School of Chemistry and Chemical Engineering, Slender West Lake Campus, Yangzhou University, Yangzhou, Jiangsu Province, P. R. China

Received May 20, 2017 / Revised June 21, 2017 / Accepted July 19, 2017

Abstract: The nitrogen (N)-doped reduced graphene aerogel (NRGA) with high *N*-doping level is successfully fabricated *via* chemical converted method and thermal activation. *N*-atoms can be incorporated at a high temperature of 900 °C and distort the lattice structure of RGA by the formation of different N-configuration bindings. NRGA exhibits a larger surface area than GA, and the surface morphology is roughened as characterized by microscopic analysis. As confirmed by X-ray photoelectron spectroscopy (XPS) result, the pyridinic- and/or pyrrolic-N bindings modified electronic structures to improve the electrochemical properties. The specific capacitance of NRGA is increased to 289 F g^{-1} at 10 mV s^{-1} with rate capability of 75% and cyclic stability of 86%. These excellent electrochemical performances of NRGA are due to the synergistic structure effect which provide a large accessible area and rapid ion transfer pathways, as well as N-containing groups acting as the electrochemical active sites positioned at the edge or on-plane of NRGA lattices.

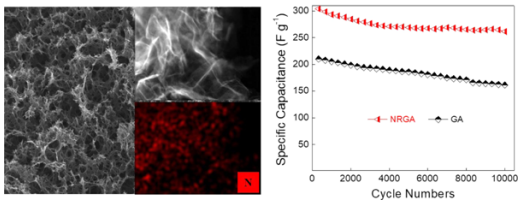

Keywords: graphene, supercapacitor, electrode, heteroatom, nanostructure.

1. Introduction

Recently, the enormous consumption of the fossil fuel for the use of our daily life, like transportion by hybrid electric vehicles, has caused a serious environment problem, which accelerated the demand for energy devices with high power density. Supercapacitor, as called electrical double layer capacitors (EDLC), can store/release energy based on the electrostatics interactions of ions at electrode and electrolyte interface, which allows supercapacitor to possess the unique properties such like high power energy, fast rate capability and long cyclic life in various applications.[1,2] Therefore, supercapacitors have attracted the attention as a promising candidiate to meet the demand of fast growth of applications. According to the capacitive properties, supercapacitors can be separated to two types: 1) EDLC, which store charges at of electrode and electrolyte interface, 2) pseudocapacitance, which can be formed by the highly reversible surface or near surface faradaic reactions. To solve the low power density of supercapacitor, the pseudocapacitive materials like metal oxide[3-5] and conducting polymers[6-9] are applied in the electrode material. However, their electrochemical performance is still un-satisfied the practical applications due to the poor electrical conductivity of metal oxide and poor cycle life of conducting polymers.

Alternatively, the incorporation of heteroatoms into carbonaceous materials can modify the electronic structure and surface chemistry, which has been demonstrated by the theoretical and experimental studies[10-12] B- or N-doped and defective graphenes. Single or binary-atoms (N, S, O, and P) have been successfully incorporated into the carbon nanomaterials lattices for a various practical applications such as oxygen reduction reaction (ORR),[13-15] lithium ion batteries,[16-18] solar cells,[19,20] and supercapacitors.[21-23] As demonstrated by lectures, the fabrication and application of nitrogen (N)-doped carbonaceous materials is of crucial importance. As a consequence of the difference of electronegativity of N and carbon is small to offer provide charge transfer in several N-containing groups. The structure of graphene can be disrupted with N atoms incorporation and open the band gap of graphene to form the defects and electro-active sites by the disruption of the electronic cloud balance of graphitic lattice by different bond angle and length. Simultaneously, the charge transfer resistance between the electrolyte and electrode can be decreased by the non-electron-neutral sites, which is benefit to enhance the capacitive performance and electrochemical behavior of carbonaceous material because of the additional contributions from the pseudocapacitance and enhanced electroconductivity.[24,25]

Herein, we have successfully synthesized the three-dimensional nitrogen incorporated reduced graphene oxides aerogel (NRGA) used as high performance supercapacitor electrodes *via* a chemical converted method. Ultimately, the porous structure of NRGA can provide a high accessible area by 3D interconnected macropores owing to self-assembly of graphene skeletons and mesopores arising from the heteroatoms incorporation with graphene lattices. Meanwhile, it is also beneficial to ion diffusion behavior and charge transfer to decrease the

Acknowledgments: This work was supported by Korea Electric Power Corporation (KEPCO, No.R17XH01).

***Corresponding Author:** Ho Seok Park (phs0727@skku.edu)

electronic resistance of the electrode and can be well wetted by the electrolyte, which may be corresponded to the surface modification of graphene. The as-prepared supercapacitor exhibits an excellent supercapacitive behavior such like high specific capacitance of 304 F g^{-1} and capacitance retention of 86% due to the additional redox activity (or pseudocapacitance).

2. Experimental

2.1. Synthesis of NRGA

The high quality of graphene oxides (GOs) dispersion were prepared and demonstrated by previous papers, which following the modified Hummers method.[26,27] The homogeneous dispersion is an important factor to form the hierarchical structure with uniform distribution of pores. Firstly, 40 mg of GOs was mixed with 7.6 mL of DI water as the solvent and ultrasonicated 30 min to make homogeneous GOs dispersion. The mixture of GO and urea with a mass ratio of 20:1 noted as solution A. The reduction agent is consist of 6.3 mL an aqueous hydrophosphorus acid and 400 mg Iodine, noted as solution B. Solution A and solution B are mixed under ultrasonication, and subsequent transferred to oven at 80 °C. After 10 h, the urea-modified graphene hydrogel was formed and it was washed by ethanol/water (v/v=1:1) solution until the solvent was neutral to get the graphene hydrogel. The hydrogel was solidified by liquid nitrogen for three days to obtain the aerogel. It is a key step for nitrogen incorporated with graphene by high temperature thermal treatment. The as-obtained aerogel was transferred to tube furnace and heated at 900 °C under Ar atmosphere (flow rate=100 cc min^{-1}. The heating rate was 10 °C min^{-1} and holding time 1 h). After heating, NRGA was obtained with cooling the system to room temperature. Reduced graphene oxides aerogel (RGA) without urea was prepared by the same method. The nitrogen doped graphene film (NGF) is fabricated by vacuum filtration with same concentration and thermal treatment with the same condition of NRGA.

2.2. Electrochemical measurements

The electrochemical behavior was firstly characterized by CV measurements by a three electrode configuration. The NRGA material acts as a working electrode, Ag/AgCl as reference electrode, and Pt wire as a counter electrode. The fabrication of working electrode as follows: 2 mg of the NRGA was attached on the Ti substrate acting as current collector. This electrode was dried in a vacuum oven at 80 °C overnight to remove the solvent and then used as working electrode. The NRGA film was cut into rectangular shape with the mass of 2.2 mg and paste on the titanium substrate. Galvaostatic charge/discharge curves were carried out at a specific current from 1 A g^{-1} to 30 A g^{-1}. The specific capacitances of electrode were calculated using the following equation:

$$C_S = I/m(\Delta V/\Delta t)$$

where I, m, and $\Delta V/\Delta t$ are the applied current density, the mass of electrode, and the discharge slope after IR drop, respectively. The electrochemical impedance spectroscopy was evaluated with a frequency range from 10^6 to 10^{-2} Hz at the amplitude of 10 mV.

2.3. Characterization

Transmission electron microscopy (TEM) images were collected on a JEM-3010 HR TEM (300 kV). SEM images were obtained using a field emission scanning electron microscope (Philips SEM 535M), equipped with a Schottky-based field emission gun. The Brunauer-Emmett-Teller (BET) were measured at 78 K using BELSORP-mini analysis program by nitrogen adsorption desorption. *In situ* Raman scattering was performed on a Jasco-Raman spectrometer with excitation by 520 nm laser light. X-ray photoelectron spectroscopy (XPS) data were obtained using a Thermo MultiLab 2000 system with an Al-Mg α X-ray source. The electrochemical characteristics of SC devices were evaluated by CV curves using a CHI 760D electrochemical workstation (CH Instruments) at room temperature. In addition, galvaostatic charge/discharge and impedence spectroscopy measurements were performed using a Solartron 1260.

3. Result and discussion

3.1. Preparation of NRGA

As illustrated in Figure 1, the uniform urea modified graphene oxides dispersion was prepared by ultrasonication and then mixed with as-prepared reduction agent mixture. The homogenous mixture was transferred to oven for 10 h to construct the three dimensional structured hydrogel. The construction of 3D hierarchical structure is attributed to the π-π configuration of RGO sheets and the hydrogen bonding between the function groups -NH of urea and -COOH of GO. The hydrogel was solidified by liquid nitrogen and freeze-dried to remove the DI water from solid phase to gas phase. After 3 days, the as-obtained aerogel was activated at 900 °C for 1 h. During the subsequent ther-

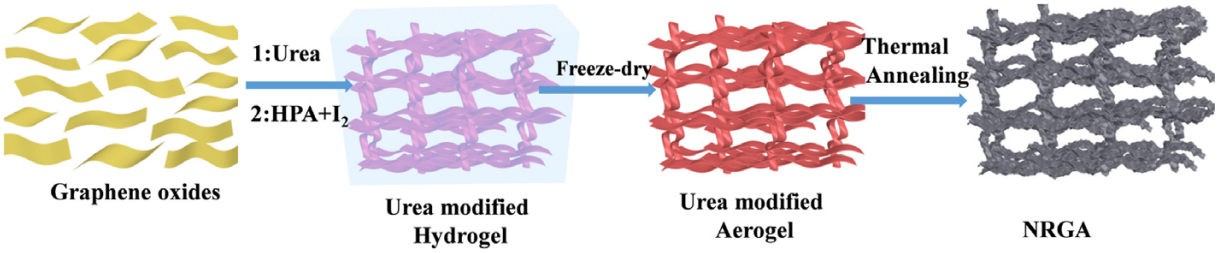

Figure 1. Illustration of synthetic procedure of NRGA with urea as the nitrogen precursor.

mal annealing process, the urea was decomposed and element nitrogen was incorporated into the graphene frameworks.

3.2. Morphology of NRGA

As shown in Figure 2, the morphology of NRGA is evaluated by scanning electron microscopy (SEM), transmission electron microscopy (TEM), and scanning TEM (STEM) images. An interconnected framework of NRGA is formed with the macropore size of few hundred nanometers to several micrometers. The graphene sheets show distinctly wrinkled feature, and was further demonstrated by TEM image (Figure 2(c)). This partially crinkled feature reduced by the defects in the NRGA and the defective structure generated due to the different bond length and angle when nitrogen atom was successfully incorporated with graphene lattices.[28] Meanwhile, the crumpled structure also can provide a large amount of exposed active sites, which is favorable for improving the electrochemical properties of supercapacitor. Figure 2(d) shows the STEM images and different elemental (C, N, O) mapping images, which reveal that the existence of element N in NRGA sample is uniformly distributed. This result demonstrate that the atoms have successfully incorporated to the graphitic lattices.

The surface area and pore structure of NRGA is also significantly affected by the heteroatom nitrogen doping. The surface area of NRGA was investigated by BET technique, and the corresponding data was listed in Table 1. As shown in Figure 3, NRGA exhibits the mesoporous structure with a typical type IV isotherm. The surface area of NRGA is 370 $m^2 g^{-1}$, which is 1.3 times greater than that of GA (285 $m^2 g^{-1}$), and the average mesopore size distribution of NRGA is 9.83 nm. The increased surface area and pore volume are attributed to the variation of bond length and bond angle and structural defect by the formation of N-containing groups. These morphology results predicted that NRGA can show an enhanced electrochemical performance.

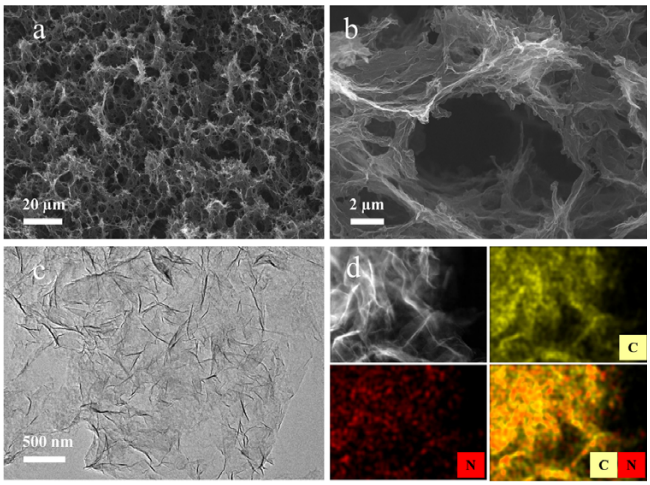

Figure 2. (a) and (b) Low and high magnification SEM images of NRGA. (c) TEM image of NRGA. (d) STEM and C, N elemental mapping images of NRGA.

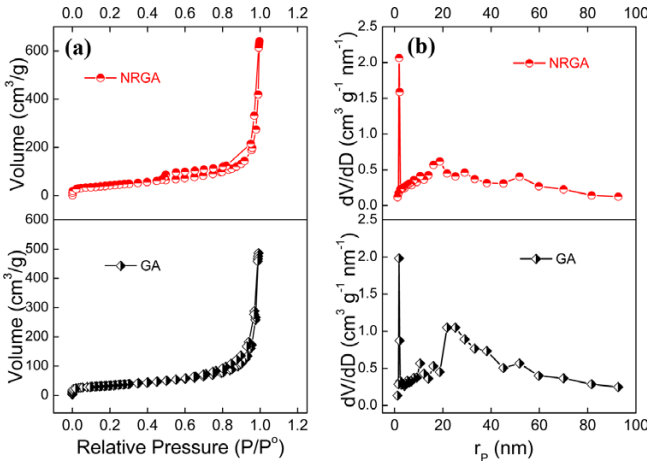

Figure 3. (a) N_2 adsorption/desorption isotherm of NRGA and GA. (b) Barrett-Joyner-Halenda (BJH) pore size distribution of NRGA and GA.

3.3. The structure and chemical composition of NRGA

The chemical nature of NRGA is further evaluated by the XPS (Figure 4). The full XPS spectra of NRGA shows three predominant peaks at 532 eV, 284 eV, and 400 eV, which are corresponding to O1s, C1s, and N1s.[29] This result demonstrated that the NRGA is consist of carbon, nitrogen and oxygen elements with the corresponding atomic ratio of 90.6%, 2.5%, and 6.9%, respectively. The nitrogen doping can distorted the sp^2-carbon network and result an improvement of the electrical conductivity of the samples. The detailed information about the bond configuration and chemical structure for NRGA are demonstrated by fitting analysis of N1s spectra. The carbon peaks can be fitted to three peaks at 284.5 eV, 286.3 eV, and 287.7 eV, which are contributed to C-C, C=N, and C-N bonding, respectively.[13] The existence of C-N and C=N bond demonstrated the successful nitrogen incorporation into grapheme lattices. The high resolution of N peak reveals that three N-containing chemical bonding are formed during the thermal treatment (Figure 4(c)). The existence of pyridinic-N at 398.3 eV is mainly exist at the edge site of graphene plane, the formation of pyrrolic-type N at 399.5 eV is contributed to the π system, and graphitic-N at 401.8 eV is also called substituted nitrogen in which nitrogen is bonded to graphene layer to take place of the C on plane of graphene. The oxide pyridinic-N at 405.8 eV is corresponding to one nitrogen atoms bonding with two carbon and one oxygen atoms. As demonstrated by recent studies, the pyridinic-N and/or pyrrolic-N are domain N-containing group as the electrochemical active site for enhanced electrocatalytic active sites.[30,31]

Table 1. Average mesopore sizes, surface areas, pore volumes, and isotherm types of GA and NRGA

Sample	Surface area ($m^2 g^{-1}$)	Pore volume ($cm^3 g^{-1}$)	Average mesopore size (nm)	Types of isotherm
GA	285	64.2	12.25	IV
NRGA	370	90.1	9.83	IV

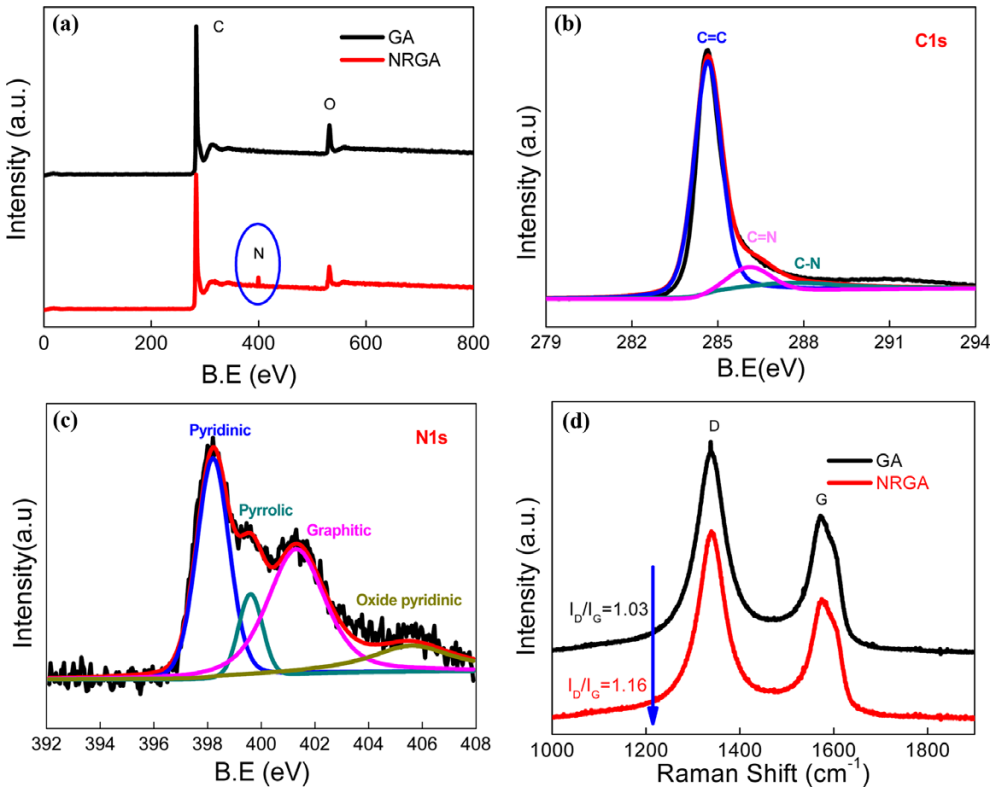

Figure 4. (a) Full scan of XPS spectrums of GA and NRGA. (b) and (c) High resolution deconvoluted peaks of C1s and N1s of NRGA. (d) Raman spectra of GA and NRGA.

Raman spectra of NRGA result was further applied to demonstrate the presence of defect sites in Figure 4(d). The peak at 1340 cm^{-1} is corresponding to the D band associating with the sp^3 distorted sites and and 1580 cm^{-1} is attributed to G band reducing by the stretching of the sp^2 bond[32,33] The slightly down-shift of bands (D, G) is attributed to the formation of defect sites and structure distortion by nitrogen doping. As an important factor to evaluate the defect sites, the intensity ration of I_D/I_G increased from 1.03 of GA to 1.16 of NRGA. This result indicated that the structure distortion in NRGA is increased with the degradation of crystallinity. These structure and chemical composition evidences strongly suggested that NRGA can show significant improvement of electrochemical performance due to hierarchical architecture and chemical composition of N-containing groups by the heteroatom N incorporation with graphene lattices.

3.4. Electrochemical behavior of NRGA

To probe the electrochemical behavior of NRGA, cyclic voltammetry (CV) was applied by three-electrode system in 1 M aqueous H_2SO_4 electrolyte at a potential window of 0.8 V Vs Ag/AgCl. The CV curves of NRGA and GA was measured at a scan rate of 10 mV s^{-1}, as shown in Figure 5(a). Both samples show a rectangular-like shape, but the charge/discharge current density of NRGA is higher than GA, indicating that the electrochemical conductivity of NRGA is better. For ideal capacitor, the energy should be recoverable during charging process at the operating voltage, which is corresponding to rectangular CV shape.[34] Meanwhile, the pseudocapacitors is related to the highly reversible faradaic reaction or surface redox reaction, which is reflected in the distorted rectangular shape. So the NRGA shows the capacitance by combining the EDLC with pseudocapacitance. The specific capacitance of NRGA is 289 F g^{-1} at a scan rate of 10 mV s^{-1}, which is superior to that of GA (202 F g^{-1}). As the scan rate increased by a factor of 20, the specific capacitance of NRGA is almost maintained about 216 F g^{-1} with a rate capability of 75%. The higher capacitance of NRGA than GA is corresponding to the pseudocapacitance contribution by formation of electrochemical active sites *via* nitrogen doping. In contrast to lectures, the specific capacitance of NRGA (289 F g^{-1}) is higher than the reported values for pristine graphene electrode[5,35] like graphene hydrogel (~175 F g^{-1}),[36] graphene-cellulose paper (~205 F g^{-1})[37] electrodes for supercapacitors. Structure effect and chemical composition effect play important roles to express the capacitive performance of the electrode material. Firstly, the specific capacitance of 2D NGF is 258 F g^{-1} at low scan rate of 10 mV s^{-1}, which is lower than that of NRGA. And the rate capability of NGF is also smaller than NRGA (Figure 5(d)). All these features suggested that better capacitive performance of NRGA is attributed to the hierarchical structures and chemical composition effect by heteroatom doping. The hierarchical structure can improve the wettability of the electrode and shorten charge transfer pathways, and the chemical configuration plays a dominant role to improve the electrochemical performance by providing more electroactive sites for fast surface redox reaction.

Galvanostatic charge/discharge (GCD) was employed to further verify the electrochemical behavior of NRGA within a potential window of 0.8 V at a various current density. At a low current density of 1 A g^{-1}, the GCD curve of NRGA shows a distorted triangular shape, which is due to the heteroatom incor-

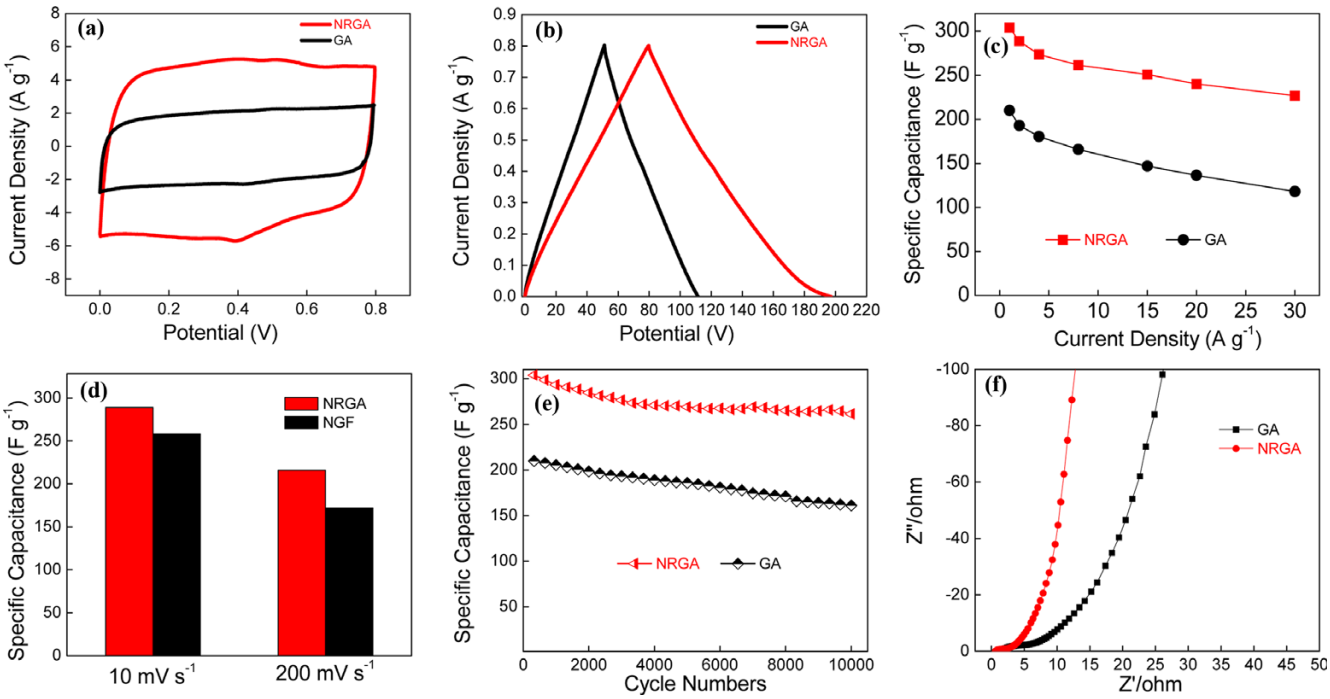

Figure 5. (a) CV curves of NRGA and GA at a scan rate of 10 mV s^{-1}. (b) GCD curves of NRGA and GA at a current density of 1 A g^{-1}. (c) Rate capability of NRGA and GA at a different current density from 1 A g^{-1} to 30 A g^{-1}. (d) The specific capacitance of NRGA and NGF at current density 10 mV s^{-1} and 200 mV s^{-1}. (e) The cyclic stability of NRGA and GA at a current density of 1 A g^{-1} for 10000 charge/discharge curves. (f) Nyquist plots of NRGA and GA.

poration with the generation of additional pseudocapacitance. As calculated by discharge curves at 1 A g^{-1}, the specific capacitance of NRGA is 304 F g^{-1}, which is 1.4 times greater than that of GA (210 F g^{-1}). And the NRGA also exhibit better rate capability than GA from current density of 1 A g^{-1} to 30 A g^{-1}, as shown in Figure 5(b). This result exhibits that NRGA has a low resistance, and the sharp decrease of the specific capacitance is attributed to the gradually decrease of the additional capacitance by the fast charge/discharge. The cyclic life of NRGA is measured by GCD at 1 A g^{-1} for 10000 cycles, as shown in Figure 5(d). After 10000 cycles, the NRGA still maintain a high specific capacitance of 262 F g^{-1} with the capacitance retention of 86%, respectively. These excellent electrochemical performance of NRGA demonstrate that the additional heteroatom N incorporation into graphene lattices can dramatically enhance the electrochemical performance due to the hierarchical structure for providing the fast electrolyte diffusion and short charge transfer pathways and the formation of electrochemical active site by the heteroatom nitrogen doping.

The electrochemical impedance spectroscopy is further used to demonstrate the electrochemical behavior. At lower frequency, NRGA shows a straightly line corresponding to an ideal capacitor (Figure 5(d)). At high frequency, the semicircle suggested the characteristic capacitive performance. NRGA shows higher slop value indicating better capacitive behavior with a low Rct corresponding to the generation of the electrochemical active sites by heteroatom doping. All these features demonstrate that the preparation of other kinds of heteroatoms such as sulfur and phosphorus can be applied as the practical energy devices due to the hierarchical effect and modification of chemical composition effect by heteroatom doping.

4. Conclusions

We fabricated the high performance supercapacitor electrode of NRGA by a urea functionalization and thermal treatment graphene aerogel. The texture and morphology are generally characterized by the SEM, STEM and TEM. The NRGA shows mesopores material property with narrow pore size distribution. The structure and chemical identifies are demonstrated by the various spectra analysis. As demonstrated by the microscopic and spectroscopic analysis, the crumpled structure and formation of N-containing groups are favorable to enhance the supercapacitive behavior of the electrode. The NRGA exhibit an improvement of the supercapacitive performance, like high specific capacitance, excellent rate and cycle stability, due to the short ion diffusion pathways of hierarchical structure and formation of the electrochemical active sites by the nitrogen doping.

References

(1) G. Wang, L. Zhang, and J. Zhang, *Chem. Soc. Rev.*, **41**, 797 (2012).
(2) C. Liu, Z. Yu, D. Neff, A. Zhamu, and B. Z. Jang, *Nano Lett.*, **10**, 4863 (2010).
(3) Y. Guo, L. Yu, C.-Y. Wang, Z. Lin, and X. W. (David) Lou, *Adv. Funct. Mater.*, **25**, 5184 (2015).
(4) X. Lang, A. Hirata, T. Fujita, and M. Chen, *Nat. Nanotechnol.*, **6**, 232 (2011).
(5) Z.-S. Wu, D.-W. Wang, W. Ren, J. Zhao, G. Zhou, F. Li, and H.-M. Cheng, *Adv. Funct. Mater.*, **20**, 3595 (2010).

(6) F. Alvi, M. K. Ram, P.A. Basnayaka, E. Stefanakos, Y. Goswami, and A. Kumar, *Electrochim. Acta*, **56**, 9406 (2011).
(7) S. Ghosh and O. Inganäs, *Adv. Mater.*, **11**, 1214 (1999).
(8) W. Jiang, D. Yu, Q. Zhang, K. Goh, L. Wei, Y. Yong, R. Jiang, J. Wei, and Y. Chen, *Adv. Funct. Mater.*, **25**, 1063 (2015).
(9) G. Qu, J. Cheng, X. Li, D. Yuan, P. Chen, X. Chen, B. Wang, and H. Peng, *Adv. Mater.*, **28**, 3646 (2016).
(10) Y.-H. Zhang, Y.-B. Chen, K.-G. Zhou, C.-H. Liu, J. Zeng, H.-L. Zhang, and Y. Peng, *Nanotechnology.*, **20**, 185504 (2009).
(11) P. Ayala, R. Arenal, M. Rümmeli, A. Rubio, and T. Pichler, *Carbon*, **48**, 575 (2010).
(12) G. Pascoli and H. Lavendy, *J. Phys. Chem. A*, **103**, 3518 (1999).
(13) C. H. Choi, S. H. Park, and S. I. Woo, *J. Mater. Chem.*, **22**, 12107 (2012).
(14) C. H. Choi, M. W. Chung, H. C. Kwon, S. H. Park, and S. I. Woo, *J. Mater. Chem. A,* **1**, 3694 (2013).
(15) S. Gao, H. Liu, K. Geng, and X. Wei, *Nano Energy*, **12**, 785 (2015).
(16) H. Wang, Z. Wu, F. Meng, D. Ma, X. Huang, L. Wang, and X. Zhang, *ChemSusChem*, **6**, 56 (2013).
(17) L. Qie, W.-M. Chen, Z.-H. Wang, Q.-G. Shao, X. Li, L.-X. Yuan, X.-L. Hu, W.-X. Zhang, and Y.-H. Huang, *Adv. Mater.*, **24**, 2047 (2012).
(18) J. Xu, M. Wang, N. P. Wickramaratne, M. Jaroniec, S. Dou, and L. Dai, *Adv. Mater.*, **27**, 2042 (2015).
(19) S. Hou, X. Cai, H. Wu, X. Yu, M. Peng, K. Yan, and D. Zou, *Energy Environ. Sci.*, **6**, 3356 (2013).
(20) X. Li, L. Fan, Z. Li, K. Wang, M. Zhong, J. Wei, D. Wu, and H. Zhu, *Adv. Energy Mater.*, **2**, 425 (2012).
(21) Z.-S. Wu, K. Parvez, A. Winter, H. Vieker, X. Liu, S. Han, A. Turchanin, X. Feng, and K. Müllen, *Adv. Mater.*, **26**, 4552 (2014).
(22) Z. Wen, X. Wang, S. Mao, Z. Bo, H. Kim, S. Cui, G. Lu, X. Feng, and J. Chen, *Adv. Mater.*, **24**, 5610 (2012).
(23) Z.-S. Wu, A. Winter, L. Chen, Y. Sun, A. Turchanin, X. Feng, and K. Müllen, *Adv. Mater.*, **24**, 5130 (2012).
(24) F. Ma, H. Zhao, L. Sun, Q. Li, L. Huo, T. Xia, S. Gao, G. Pang, Z. Shi, and S. Feng, *J. Mater. Chem.*, **22**, 13464 (2012).
(25) D. Zhang, Y. Hao, L. Zheng, Y. Ma, H. Feng, and H. Luo, *J. Mater. Chem. A*, **1**, 7584 (2013).
(26) W. S. Hummers and R. E. Offeman, *J. Am. Chem. Soc.*, **80**, 1339 (1958).
(27) B. G. Choi, W. H. Hong, Y. M. Jung, and H. Park, *Chem. Commun.*, **47**, 10293 (2011).
(28) S. Yang, L. Zhi, K. Tang, X. Feng, J. Maier, and K. Müllen, *Adv. Funct. Mater.*, **22**, 3634 (2012).
(29) W. Ai, Z. Luo, J. Jiang, J. Zhu, Z. Du, Z. Fan, L. Xie, H. Zhang, W. Huang, and T. Yu, *Adv. Mater.*, **26**, 6186 (2014).
(30) P. H. Matter, L. Zhang, and U. S. Ozkan, *J. Catal.*, **239**, 83 (2006).
(31) S. Maldonado and K. J. Stevenson, *J. Phys. Chem. B*, **109**, 4707 (2005).
(32) C. H. Choi, S. H. Park, and S. I. Woo, *ACS Nano*, **6**, 7084 (2012).
(33) L. Feng, Y. Chen, and L. Chen, *ACS Nano*, **5**, 9611 (2011).
(34) J. Lee, S. Yoon, S. M. Oh, C.-H. Shin, and T. Hyeon, *Adv. Mater.*, **12**, 359 (2000).
(35) L. L. Zhang, R. Zhou, and X. S. Zhao, *J. Mater. Chem.*, **20**, 5983 (2010).
(36) Y. Xu, K. Sheng, C. Li, and G. Shi, *ACS Nano*, **4**, 4324 (2010).
(37) K. Gao, Z. Shao, J. Li, X. Wang, X. Peng, W. Wang, and F. Wang, *J. Mater. Chem. A*, **1**, 63 (2012).